EURASIP Journal on Advances in Signal Processing

RESEARCH Open Access

Research on alleviating nonlinear problem by data feature extraction and fusion based on DFT-spread

Yupeng Li[1,2*], Lei Li[1,2], Yichao Zhang[1,2], Mingzhu Zhang[1,2], Du Wu[1,2], Qianqian Li[1,2], Xiaocheng Wang[1,2] and Xiaoming Ding[1,2]

*Correspondence: fx_lyp@163.com

[1] Tianjin Key Laboratory of Wireless Mobile Communication and Power Transmission, Tianjin Normal University, Tianjin 300387, China
[2] College of Electronic and Communication Engineering, Tianjin Normal University, Tianjin 300387, China

Abstract

Coherent optical orthogonal frequency division multiplexing (CO-OFDM) system is susceptible to nonlinear effects because of its intrinsic high peak-to-average ratio (PAPR). In this paper, two methods based on discrete Fourier transform spread (DFT-S) are introduced to improve the nonlinear tolerance of CO-OFDM system by extracting and fusing data features, which extract the features of communication data and perform feature fusion to get the important significance of the data. The first one is based on the 2-ary amplitude shift keying (2-ASK) modulation and the Hermitian symmetry of DFT, and the other one is based on the advantages of selective mapping algorithm and characteristics of data subcarrier mapping mode which has a significant impact on PAPR. Simulation results show that compared with the traditional CO-OFDM and DFT-S CO-OFDM systems, the improved methods have better performance in terms of PAPR and BER.

Keywords: DFT-S, CO-OFDM, Nonlinear tolerance, PAPR

1 Introduction

With the rapid development of communication industry, especially data service such as high-definition video, big data, broadband wireless communication and cloud computing, higher requirements are put forward for the optical transmission network [1, 2]. Because of the advantages of high polarization mode dispersion (PMD) and chromaticity dispersion (CD) tolerance, spectral efficiency and receiver sensitivity, CO-OFDM system has become one of the most promising schemes for long-distance and highspeed optical fiber transmission systems [3]. In addition, the digital signal processing (DSP) technology makes it more flexible at the transmitter and receiver [4]. For example, a variety of modulation formats and flexible subcarrier allocation are available for operation [5]. Moreover, training sequences (TS) can be inserted to perform channel estimation by zero forcing equalization (ZFE) or minimum mean square equalization (MMSE), cyclic prefix (CP) and pilots can be used as supplementary information to perform frequency offset estimation and phase estimation, respectively [6, 7].

Since OFDM symbol is superimposed by multiple independent subcarriers, its intrinsic high peak-to-average power ratio (PAPR) will cause the OFDM signal to exceed the linear range of digital analog converter (D/A), analog digital converter (A/D) and amplifier, which makes the system be affected by phase noise and nonlinear effects easily [8, 9]. In order to alleviate the fiber nonlinearity problem caused by high PAPR in CO-OFDM system, a variety of schemes for mitigating fiber nonlinear effects have been proposed, such as clipping, peak windowing and peak offset, predistortion, SLM, Convex Optimization [10], and constant envelope (CE) OFDM [11]. However, these schemes have some disadvantages in system performance, computational complexity and spectral efficiency. Therefore, comprehensive performance evaluation is necessary when mitigating the nonlinear effect of CO-OFDM system. Apart from above methods, spread techniques such as Carrier Interferometry (CI) codes, Walsh Hadamard (WH) codes and DFT-Spread can effectively reduce PAPR without low computational complexity and increasing bit error rate. However, DFT-Spread is commonly used in reducing PAPR and computational complexity of OFDM systems due to its simple and easy to understand characteristics [12–17]. Based on this, improving the nonlinear tolerance of next-generation CO-OFDM system has become a key research topic [18–20].

The OFDM system based on DFT-S spread the spectrum of each modulation symbol to the entire bandwidth for transmission. Thus, the high peak value signal formation probability of OFDM signal can be reduced effectively, so as to reduce the PAPR and increase the nonlinear tolerance of OFDM system in transmission.

In this paper, we analyzed and studied two CO-OFDM systems based on DFT-S, which reduce PAPR in two aspects: symbol mapping modulation and subcarrier mapping. First, a novel 2-ASK DFT-S with Hermitian symmetry CO-OFDM (2-ASK DFT-S CO-OFDM) system was introduced. By combining the DFT-S operation and the Hermitian symmetry, the PAPR of 2-ASK DFT-S CO-OFDM system has been reduced significantly. Second, a method of selective mapping of interpolated subcarrier based on DFT-S (SLM DFT-S) was introduced to reduce PAPR by regularly changing the subcarrier interpolation mapping modes, which has better signal fidelity and nonlinear tolerance. The important influence of subcarrier mapping mode on transmission performance in OFDM system was also verified. Different from the first method, the SLM DFT-S CO-OFDM keeps 4-QAM unchanged, and generates a variety of OFDM symbol samples to choose the one with smallest PAPR for transmission.

The rest of this study is structured as follows. The signal transmission process of the traditional CO-OFDM and DFT-S CO-OFDM systems is described in Sect. 2. Both principle and structure of the introduced systems are presented in Sect. 3. We establish simulation system and analyze the results in Sects. 4 and 5. Section 6 is conclusion.

2 The system models of traditional CO-OFDM and DFT-S CO-OFDM

Figure 1 shows the signal flow diagram of the traditional CO-OFDM system. First, the pseudo-random binary sequence is processed by 4-QAM mapping. After that, series-to-parallel (S/P) conversion and subcarrier mapping are carried out and then the training sequence is inserted for frequency offset and channel estimation. Assuming that the data sequence before N-point inverse FFT (IFFT) is $x = [x_0, x_1, \ldots, x_{N-1}]^T$. The transmitted OFDM signal after IFFT in the time domain is given as

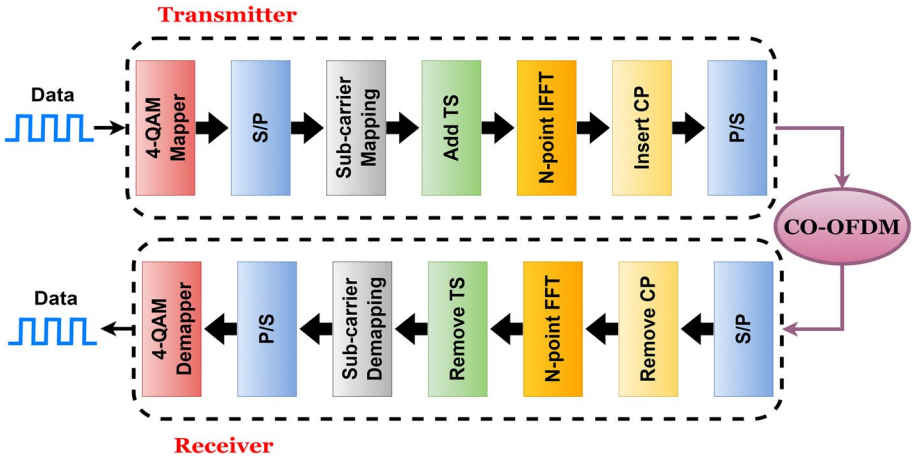

Fig. 1 Signal flow diagram of the traditional CO-OFDM system

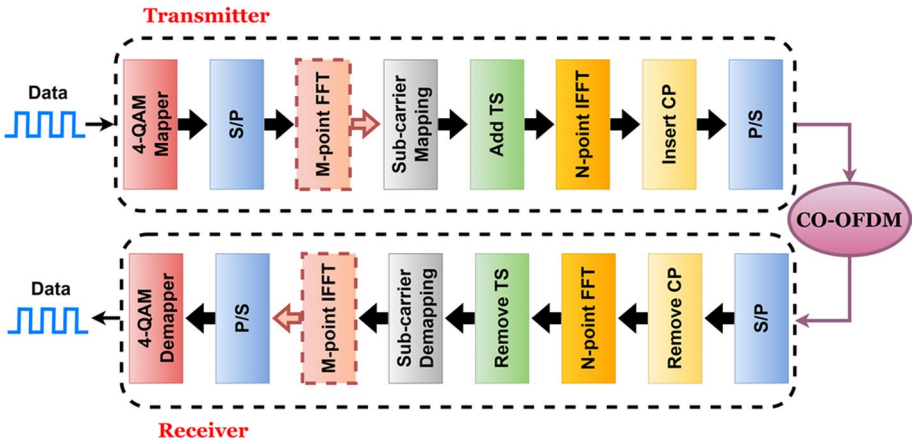

Fig. 2 Signal flow diagram of the DFT-S CO-OFDM system

$$S_t = \frac{1}{\sqrt{N}} \sum_{k=0}^{N-1} x_k \cdot e^{j2\pi \frac{k}{N} t}, \quad (0 \le t \le N-1) \tag{1}$$

where N is the size of IFFT.

After parallel to series (P/S) conversion and cyclic prefix (CP) insertion, the data are ready for optical modulation. At the receiver, the original data are recovered by the opposite operations of the transmitter.

Figure 2 is the signal flow diagram of 4-QAM DFT-S CO-OFDM system. Different from the traditional OFDM system, an additional M-point FFT operation is performed before subcarrier mapping, and the output can be expressed as

$$X_k = \sum_{q=0}^{M-1} x_q \cdot e^{-j2\pi \frac{q}{M} k}, \quad (0 \le k \le M-1) \tag{2}$$

where $x = [x_0, x_1, \ldots, x_{M-1}]^T$ is the data before FFT and M is the FFT size.

The spread spectrum data are then formed into OFDM signal through subcarrier mapping and IFFT:

$$S_t = \frac{1}{\sqrt{N}} \sum_{k=0}^{N-1} X_k \cdot e^{j2\pi \frac{k}{N} t}, \quad (0 \le t \le N-1) \tag{3}$$

where N is the IFFT size.

It is worth mentioning that M should be less than N. Similarly, the reverse operations are performed at the receiver to recover original data. Compared to the traditional system, only a pair of FFTs is added, but the nonlinear tolerance is enhanced significantly [21–26]. Therefore, the research based on this system is also worth exploring, which is an important theoretical basis for the methods studied in this paper.

3 The system models of 2-ASK DFT-S CO-OFDM and SLM DFT-S CO-OFDM

3.1 2-ASK DFT-S CO-OFDM system

The signal flow diagram of the 2-ASK DFT-S CO-OFDM system is illustrated in Fig. 3. Different from two systems described above, this system adopts 2-ASK symbol mapping modulation and uses Hermitian conjugate symmetry to further reduce PAPR without changing the amount of data despite the lower band utilization than 4QAM. The pseudo-random binary sequence input is mapped into 2-ASK symbols and then the M-point FFT is performed after S/P conversion. Subsequently, the data sequence is spread across the entire bandwidth through M-point FFT:

$$X_k = \sum_{q=0}^{M-1} x_q \cdot e^{-j2\pi \frac{q}{M} k}, \quad (0 \le k \le M-1) \tag{4}$$

As shown in Fig. 4, all subcarriers except direct current (DC) subcarrier and Nyquist subcarrier are symmetric after FFT because of the Hermitian symmetry. The redundant subcarriers are removed to avoid wasting bandwidth, and only $M/2+1$ data subcarriers are processed with IFFT [27, 28]. The research system reduces the symbol

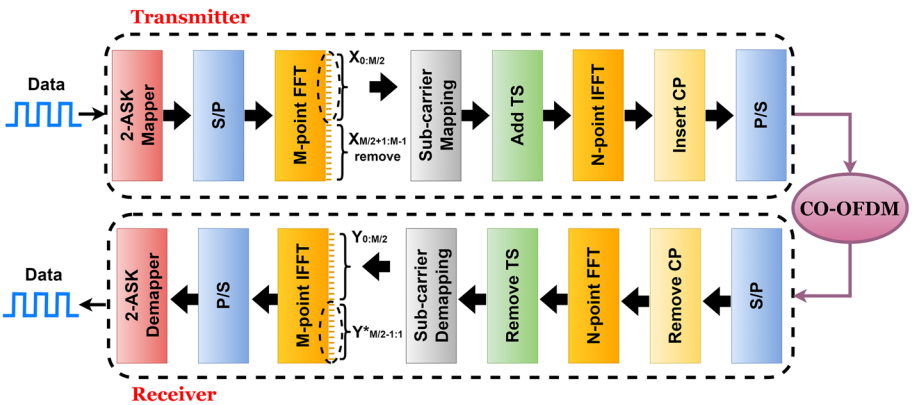

Fig. 3 Signal flow diagram of the 2-ASK DFT-S CO-OFDM system

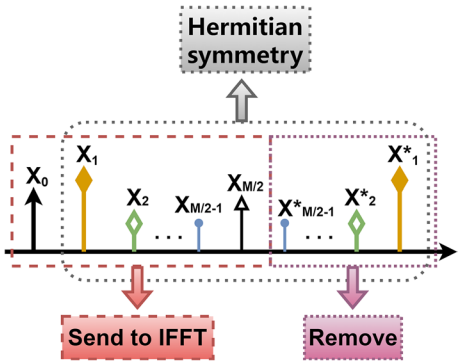

Fig. 4 The Hermitian conjugate symmetry of DFT

mapping order from 4 to 2, and increases the size of FFT to maintain the same data rate [29]. Zero subcarriers are supplemented before IFFT, which can be expressed as

$$\tilde{X}_k = \begin{cases} X_k, & \left(0 \le k \le \frac{M}{2}\right) \\ 0, & \left(\frac{M}{2} + 1 \le k \le N\right) \end{cases} \tag{5}$$

where M and N are the sizes of FFT and IFFT, respectively.

In addition to the data subcarriers, several subcarriers are reserved as the pilot subcarriers, which are not expressed in the formula because of the complexity of the representation. Then the OFDM signals can be obtained by IFFT after zero filling as

$$S_t = \frac{1}{\sqrt{N}} \sum_{k=0}^{N-1} \tilde{X}_k \cdot e^{j2\pi \frac{k}{N} t}, \quad (0 \le t \le N-1) \tag{6}$$

Accordingly, the received signal performs the opposite N-point FFT at the receiver:

$$Y_t = \sum_{r=0}^{N-1} S_r \cdot e^{-j2\pi \frac{r}{N} t}, \quad (0 \le t \le N-1) \tag{7}$$

The Hermitian symmetry is then used to recover the signal as

$$\tilde{Y}_t = \begin{cases} Y_t, & \left(0 \le t \le \frac{M}{2}\right) \\ Y_t^*, & \left(\frac{M}{2} + 1 \le t \le M-1\right) \end{cases} \tag{8}$$

In Eq. (8), the duplicate data are removed by the transmitter can be completely recovered. Therefore, the signal after M-point IFFT is as follows

$$R_k = \frac{1}{\sqrt{M}} \sum_{d=0}^{M-1} \tilde{Y}_t \cdot e^{j2\pi \frac{d}{M} k}, \quad (0 \le k \le M-1) \tag{9}$$

3.2 SLM DFT-S CO-OFDM system

The signal flow diagram of the SLM DFT-S CO-OFDM system is shown in Fig. 5. All data carriers are divided into M/L parts. Assuming $K = M/L$, then M valid data are divided into K frequency bands. After L-point FFT is carried out for each sub-band,

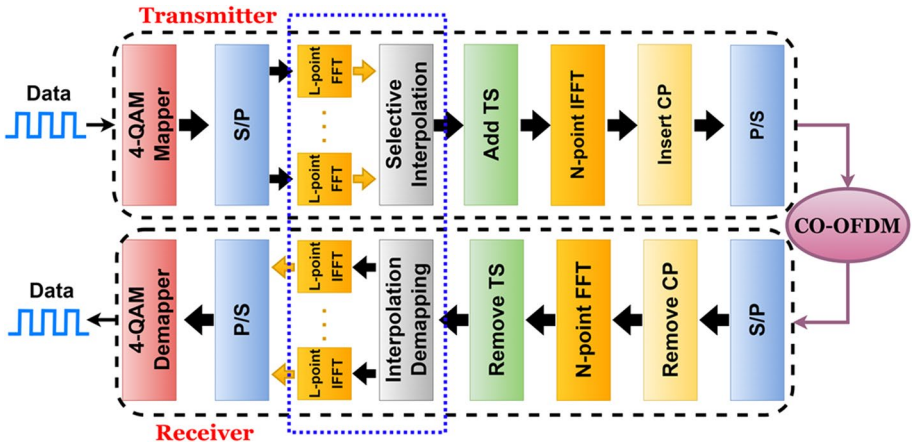

Fig. 5 Signal flow diagram of the SLM DFT-S CO-OFDM system

subcarrier interpolation mapping is carried out according to certain rules [30]. Then appropriate phase factors are selected for different mapping methods to form different OFDM signals, and finally the signal with lowest PAPR is selected to transmit [31].

$$x_n = \frac{1}{N}\sum_{p=0}^{N-1} X_p e^{j2\pi np/N} = \frac{1}{K\times M}\sum_{q=0}^{M-1} X_q e^{j2\pi nq/M} = \frac{1}{K}x_m \tag{10}$$

In Eq. (10), N, K and M denote the number of total subcarriers, subbands and subcarriers in single subband, respectively, and $N=K\times M$. The x_n and x_m are the output and input symbol of IFFT respectively. Weighting the equalization signal x_n obtained. If the dimension is N, the weighting process through linear conversion is expressed as

$$x_n^{'} = K_n \cdot x_n, \quad (0 \le n \le N-1) \tag{11}$$

The signal with the lowest PAPR is obtained by selecting appropriate K sequence, which can be defined as:

$$K_n = e^{j\theta_n}, (\theta_n \epsilon [0, 2\pi], 0 \le n \le N-1) \tag{12}$$

The output after M/L FFTs is

$$X_{kL+l} = \frac{1}{K}x_l, (0 \le l \le L-1, 0 \le k \le K-1) \tag{13}$$

As shown in Fig. 6, various mapping schemes can be obtained through subcarrier interpolation mapping. Two of the most widely known schemes are localized allocation and distributed allocation, which are defined by the degree of aggregation of data subcarriers in the same frequency band. Appropriate training factors can be selected by each mapping scheme to form multiple OFDM signals. Assuming P is mapping schemes and V is random sequences of training factors, $P\times V$ OFDM symbols is generated as [32]:

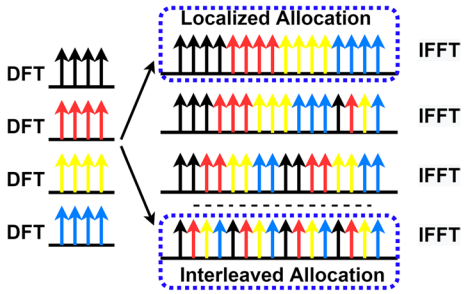

Fig. 6 Schematic of selective interpolation mapping

$$\begin{aligned} X_N^p &= \left(X_N^0, X_N^1, \ldots, X_N^{P-1}\right), \ (0 \le p \le P-1) \\ \theta_N^v &= \left(\theta_N^0, \theta_N^1, \ldots, \theta_N^{V-1}\right), \quad (0 \le v \le V-1) \end{aligned} \tag{14}$$

where the size of IFFT is N. Then the OFDM symbol set can be generated:

$$U_N^{P\times V} = \left(X_N^p \cdot \theta_N^0, X_N^p \cdot \theta_N^1, \ldots, X_N^p \cdot \theta_N^{V-1}\right), \quad (0 \le v \le V-1) \tag{15}$$

The PAPR of the set $U_N^{P\times V}$ is compared and the sequence with the minimum value is chosen to generate the OFDM signal.

4 Simulation setup

Figure 7 is the simulation setup to explore the transmission performance of above CO-OFDM systems. For traditional CO-OFDM, DFT-S CO-OFDM and the SLM DFT-S CO-OFDM systems, 4-QAM is used for symbol mapping, while 2-ASK is used for the 2-ASK DFT-S CO-OFDM system.

The traditional CO-OFDM, DFT-S CO-OFDM and the SLM DFT-S CO-OFDM systems have 128 data subcarriers and ultimately complete 256-point IFFT at the transmitter. The remaining subcarriers are supplemented by zero subcarriers and pilot subcarriers. 256-point FFT is employed in the 2-ASK DFT-S CO-OFDM system, while the SLM DFT-S CO-OFDM system uses eight 16-point FFTs to complete the signal spreading.

In 2-ASK DFT-S CO-OFDM system, the FFT size is twice as large as the other systems at 256 to maintain the same amount of data, and the size of the valid data sequence of 129 is obtained by removing redundant data. The size of IFFT after subcarrier mapping is 256. The SLM DFT-S CO-OFDM system divides the 4-QAM symbol sequence of size 128 into 8 subbands for 16-point FFT, respectively, and then 256-point IFFT is performed after sub-carrier interpolation mapping. In addition, the pilots, CP, and the training sequence are added to compensate the signal damage caused during optical transmission. The digital-to-analog converter (DAC) transforms the transmitted OFDM signal to analog signal at the sampling rate of 20 GS/s. Then, the modulated optical OFDM signal is obtained by driving optical in-phase/quadrature (I/Q) modulator.

The erbium-doped fiber amplifier (EDFA) and optical attenuator are used to adjust the optical signal power into the fiber. The parameter properties of standard

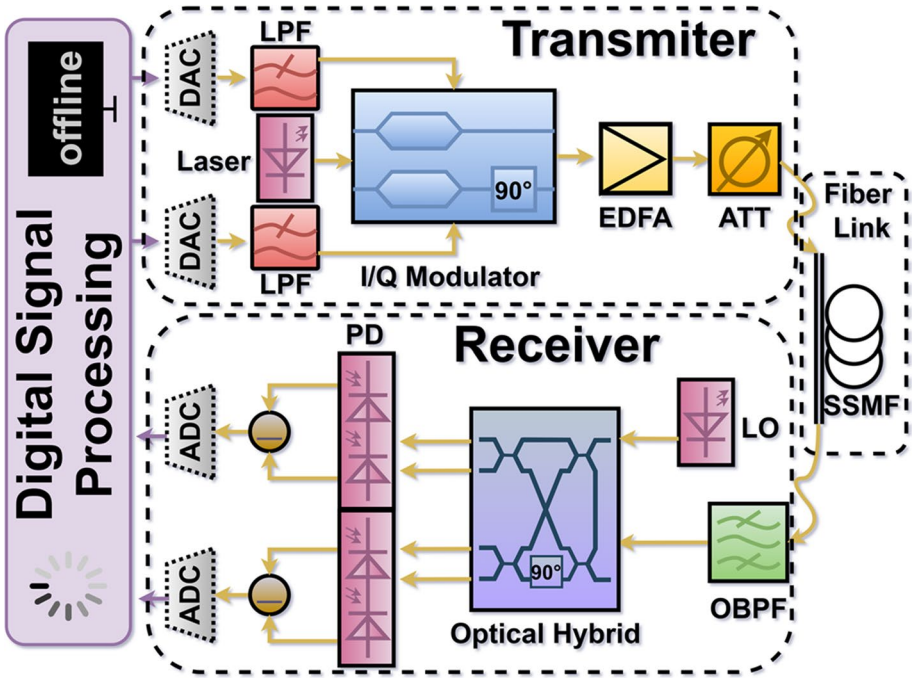

Fig. 7 Simulation setup of the CO-OFDM system. *DAC* Digital-to-analog converter; *LPF* Low pass filter; *EDFA* Erbium-doped fiber amplifier; *ATT* Attenuator; *SSMF* Standard single mode fiber; *LO* Local oscillator; *OBPF* Optical bandpass filter; *PD* Photodiode; *ADC* Analog to digital converter

Table 1 Parameter setting of simulation system

Key parameters of SMF	Value
Length of fiber	100 km
Dispersion coefficient	16 ps/nm/km
Nonlinear index	2.6e-20 m^2/W
Attenuation coefficient	0.2 dB/km
Effective core area	80e-12 m^2
IFFT/FFT point	256
Launch power	3–10 dBm
Received power	— 9–1 dBm
Bandwidth	20 GHz
SNR	22 dB

single-mode fiber (SSMF) are shown in Table 1. In order to observe the effects of dispersion, nonlinearity and attenuation in the SSMF, the diffusion of the optical signal over the long-distance fiber is simulated by solving the nonlinear Schrodinger equation, which can be solved by the split-step Fourier method (SSFM).

In the detection part of CO-OFDM system, the OFDM signal is detected by the optical coherent detector which is composed of a locally oscillating laser (LO laser), an optical 90° hybrid and two balanced photoelectric detectors (BPD). The original data are recovered through subsequent DSP processing.

5 Results and discussion

Figure 8 depicts the electrical waveform of the CO-OFDM systems. The color of the waveform indicates a gradual increase in amplitude from red to purple, the positive thresholds and signal peaks are also marked. Compared with DFT-S CO-OFDM, 2-ASK DFT-S CO-OFDM and SLM.

DFT-S CO-OFDM have smoother signal distribution, indicating a significant improvement in reducing PAPR. The 2-ASK DFT-S CO-OFDM system obviously performs better in reducing PAPR and has a very average signal amplitude distribution, which is about 1 dB lower than SLM DFT-S CO-OFDM, and nearly 4.2 dB less than the traditional CO-OFDM system.

All four systems have the same data rate and spectral efficiency, 17.78 Gb/s and 3.56 bit/s/Hz. The computational complexity of the traditional CO-OFDM system is $(N/2)\times\log_2 N$ multiplications and $N\times\log_2 N$ additions. Because of the extra FFT and IFFT, the computational complexities are $(M/2)\times\log_2 M+(N/2)\times\log_2 N$ multiplications, $M\times\log_2 M+N\times\log_2 N$ additions, $M\times\log_2(2M)+(N/2)\times\log_2 N$ multiplications, $2M\times\log_2(2M)+N\times\log_2 N$ additions and $(M/2)\times log_2 L+(N/2)\times\log_2 N$ multiplications, $M\times\log_2 L+N\times\log_2 N$ additions for DFT-S CO-OFDM system, the 2-ASK DFT-S CO-OFDM system and the SLM DFT-S CO-OFDM, respectively. The 2-ASK DFT-S CO-OFDM has the highest computational complexity, while the SLM DFT-S CO-OFDM has the lower one than DFT-S CO-OFDM system.

5.1 PAPR contrast

In order to investigate the PAPR performance of each system intuitively, 500 OFDM symbols are generated at the transmitter and analytically calculated the PAPR function curve of each system. The PAPR of OFDM signal at the transmitter can be given by

$$\mathrm{PAPR}=10\lg\frac{\max|S_t|^2}{E\left[|S_t|^2\right]} \tag{16}$$

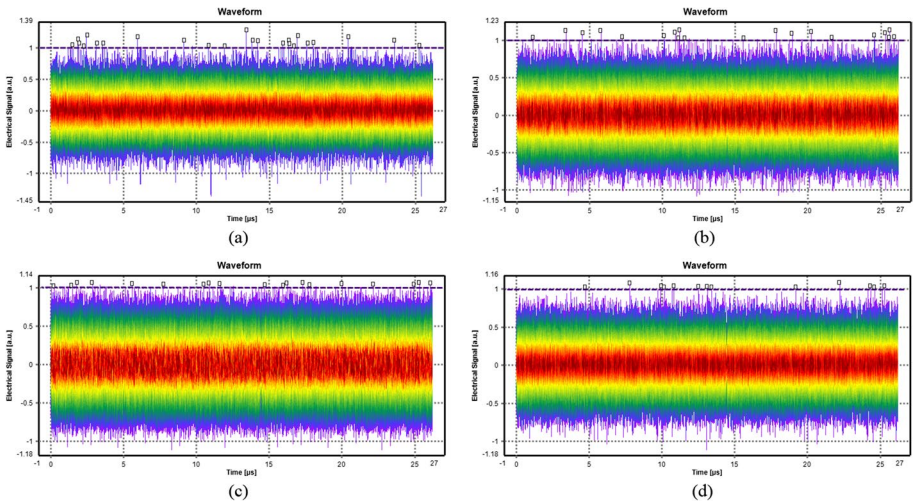

Fig. 8 Electrical waveform of **a** traditional CO-OFDM system, **b** DFT-S CO-OFDM system, **c** the 2-ASK DFT-S CO-OFDM system and **d** the SLM DFT-S CO-OFDM

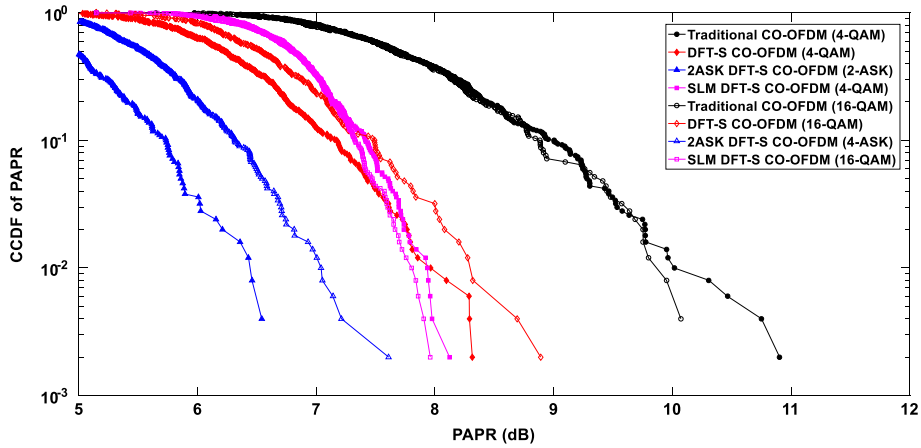

Fig. 9 CCDF of PAPR of research systems compared with the traditional CO-OFDM and DFT-S CO-OFDM systems

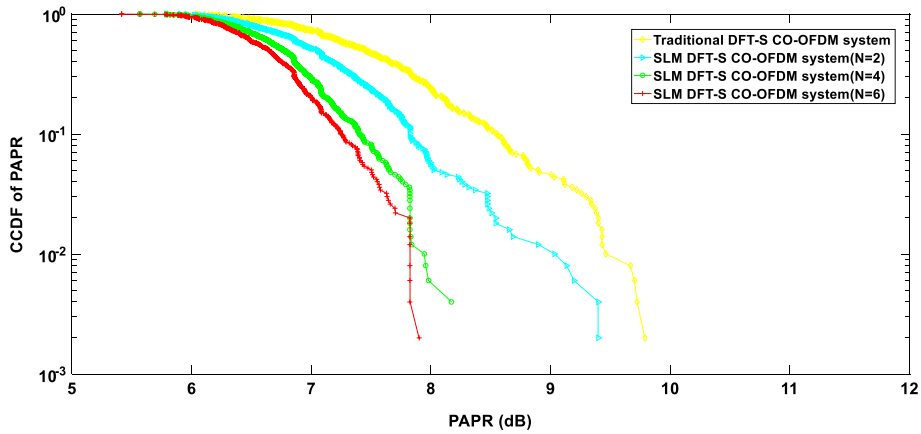

Fig. 10 CCDF of PAPR of SLM DFT-S CO-OFDM in different *N* compared with the traditional DFT-S CO-OFDM

The amplitude of traditional OFDM signal satisfies Gaussian distribution [33], while the DFT-S OFDM signal belongs to single carrier signal so that its amplitude cannot satisfy Gaussian distribution [33, 34]. The PAPR of traditional OFDM will not be influenced by *M*-order modulation, while the modulation order has a direct proportional influence on the instantaneous power distribution of DFT-S OFDM system. The instantaneous power of the signal increases with the modulation order. Therefore, reducing the modulation order of M-QAM DFT-S OFDM system can further reduce the PAPR.

The results of complementary cumulative distribution function (CCDF) of PAPR are shown in Fig. 9. Unlike other 4-QAM systems mentioned in this paper, the 2-ASK DFT-S CO-OFDM system has reduced the 4-order modulation to 2 of which the PAPR is obviously lower than other systems. The result shows that the 2-ASK DFT-S CO-OFDM system has the optimal PAPR inhibition performance with the reduction of the modulation order. Correspondingly, the same regular characteristics are also shown in 16-QAM and 4-ASK with higher modulation orders.

Figure 10 shows the PAPR performance of SLM DFT-S CO-OFDM with different amount of subcarrier interpolation. Obviously, by combining SLM method, the larger

N is, the smaller PAPR value of the system will be. In other words, the more OFDM symbol types can be selected, the better PAPR performance will be achieved. As mentioned before, this system can obtain more OFDM symbol types by adding phase factor sequence, indicating that PAPR can be reduced more significantly. Of course, there is a lower limit, and it cannot continue when it drops to a certain extent. In addition, the complexity of the system should be considered when select appropriate interpolated number. In this paper, N is set to 5, and the phase factor is only $[j, -j]$, so the system complexity is relatively not high, and the PAPR of the system is also significantly reduced compared with the traditional OFDM.

Since the principle of oversampled Carrier Interferometry (CI) CO-OFDM is similar to DFT-S CO-OFDM, corresponding PAPR comparison is carried out as a supplement. According to ref. [15], $M=2$ refers to oversampled factor and can be representative. As the comparison result shown in Fig. 11, the two investigated methods in this paper show better PAPR performance.

5.2 Transmission performance

Figure 12 is the constellation diagrams of four CO-OFDM systems after transmission. According to the color bar on the right side of the constellation diagram, the constellation points of SLM DFT-S CO-OFDM system are obviously more concentrated than that of the traditional CO-OFDM and DFT-S CO-OFDM systems, indicating fewer signal error. Moreover, the constellation of the 2-ASK DFT-S CO-OFDM system has the largest density according to the digital label of the color bar, which is also because 2-ASK does not need a complex mapping process compared with 4-QAM. As a result, the amount of data displayed on the constellation is twice that of the other systems. It can be seen clearly that the shape and divergence degree of constellation diagrams in the introduced systems are better than the traditional CO-OFDM and DFT-S CO-OFDM systems.

Figures 13 and 14 show performance of CO-OFDM systems with different launch power and transmission distance. Generally, the system performance is affected by linear and nonlinear noise. In the case that the linear noise is basically consistent, more attention should be focused on reducing the signal distortion caused by the nonlinear

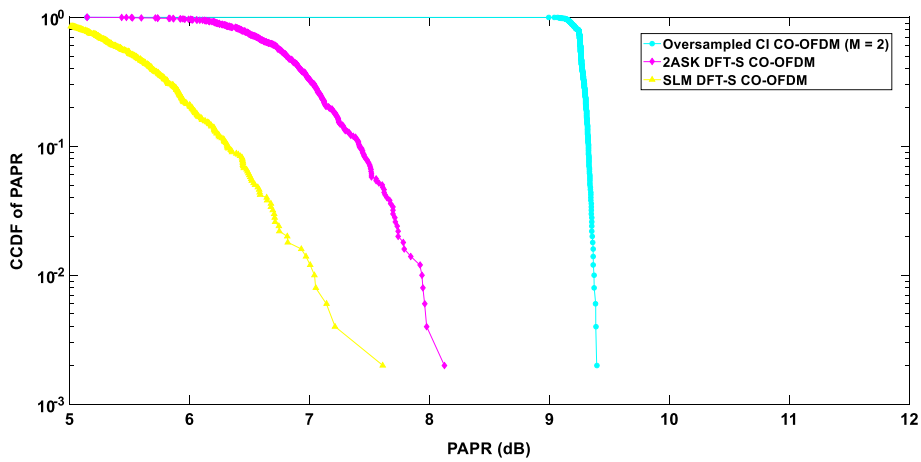

Fig. 11 CCDF of PAPR of research systems compared with oversampled CI CO-OFDM system

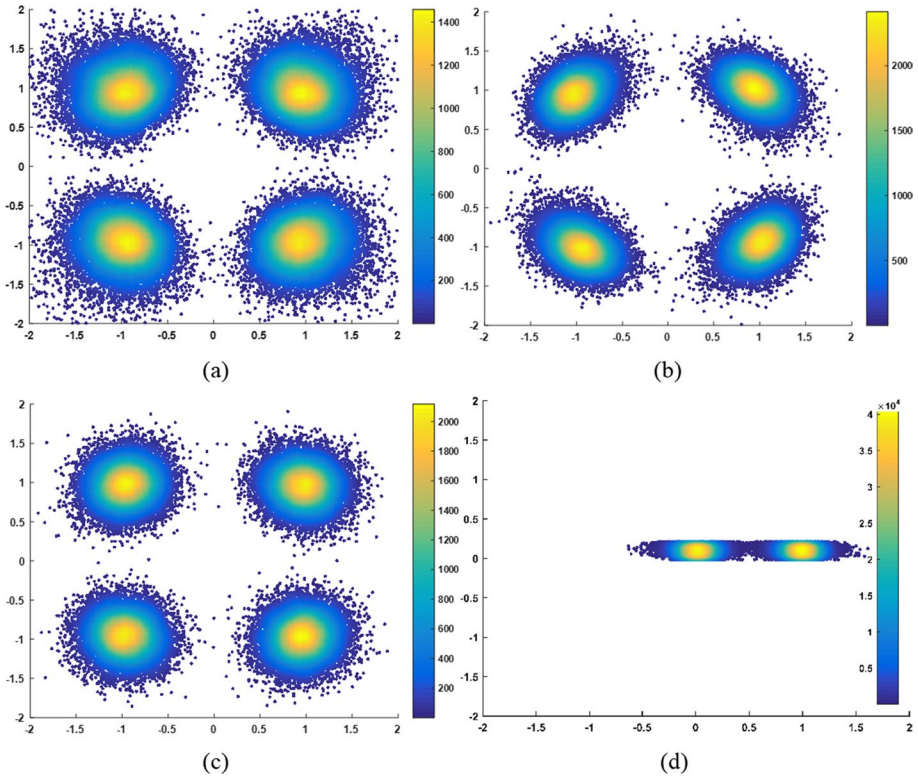

Fig. 12 Constellation diagrams of the received data after 100 km SSMF for: **a** traditional CO-OFDM, **b** DFT-S CO-OFDM, **c** the SLM DFT-S CO-OFDM and **d** the 2-ASK DFT-S CO-OFDM system

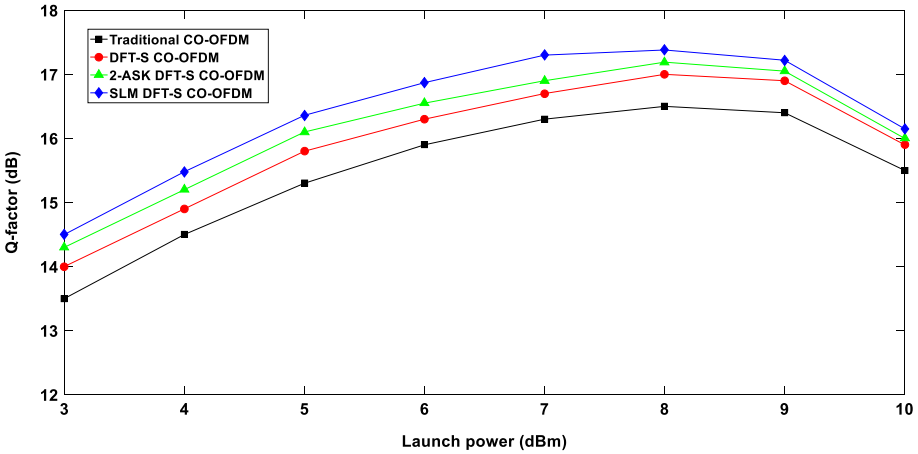

Fig. 13 The measured Q-factor versus launch power of research systems compared with the traditional CO-OFDM and DFT-S CO-OFDM systems

effect of the optical fiber. In general, the larger transmission power and longer transmission distance are, the greater nonlinear effect of the transmission system is.

As shown in Fig. 13, the gain of launch power augments the nonlinear effects. The nonlinear distortion is effectively suppressed in research systems compared to the traditional CO-OFDM and DFT-S CO-OFDM systems. When the power into fiber is 8 dBm,

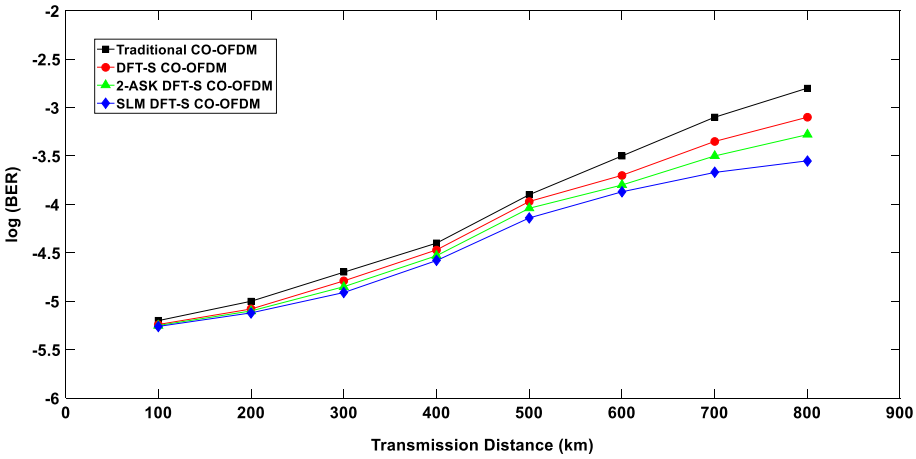

Fig. 14 log (BER) versus transmission distance for CO-OFDM systems

all systems have the highest Q value, which also means that the launch power cannot be too low or too high, otherwise the performance will be influenced by the nonlinear effect.

Similarly, as shown in Fig. 14, the BER of system increases with the increase of transmission distance. At the beginning of the transmission of all systems, the performance gap is not large. Later, the nonlinear tolerance of these systems is changed when the transmission length increases to a certain length, which is reflected in the system transmission performance gap gradually opened. Although PAPR is greatly reduced, the impact of linear noise also causes certain performance degradation. In general, the introduced systems in terms of nonlinear performance are obviously superior to the traditional CO-OFDM and DFT-S CO-OFDM systems, which are very feasible methods.

6 Conclusion

We analyzed and studied two improved schemes based on DFT-S which namely the 2-ASK DFT-S CO-OFDM system and the SLM DFT-S CO-OFDM system, and comprehensively summarized the advantages of resisting nonlinear effects. The numerical simulation results finally confirmed our prediction. Compared with the traditional CO-OFDM and DFT-S CO-OFDM systems, the improved schemes greatly reduced PAPR and effectively suppressed the nonlinear distortion of the fiber, and thus significantly improved the transmission performance of the system. In general, the research methods will play a key role in the next generation of high data rate, long distance and high spectral efficiency optical communication systems in the future.

Acknowledgements
Not applicable.

Author contributions
All authors read and approved the final manuscript.

Funding
This work was supported in part by the Natural Science Foundation of China under Grant Nos. 61901301, 62001327 and 62001328.

Availability of data and materials
Not applicable.

Declarations

Competing interests
The authors declare that they have no competing interests.

Received: 14 October 2022 Accepted: 21 February 2023
Published online: 06 March 2023

References

1. F. Wang and X. Wang, Coherent optical DFT-spread OFDM. Adv. Opt. Technol. **2011**, 689289 (2011). https://doi.org/10.1155/2011/689289
2. L. Tao, H. Tan, C. Fang, Iterative algorithm for phase noise estimation in coherent optical DFT-S OFDM systems. OE **56**, 076103 (2017)
3. G. Gao, X. Chen, W. Shieh, Analytical expressions for nonlinear transmission performance of coherent optical OFDM systems with frequency guard band. J. Lightwave Technol. **30**, 2447 (2012)
4. F. Li, Z. Cao, G. Wen, J. Xiao, J. Yu, L. Chen, Optimization of pilot interval design in direct-detected optical OFDM system. Opt. Commun. **285**, 3075 (2012)
5. X. Fang, Y. Wang, D. Ding, L. Zhang, and C. Zhao, Pilot-aided phase noise suppression for coherent optical OFDM/OQAM, in *2019 Asia Communications and Photonics Conference (ACP)* (2019), pp. 1–3
6. A. Trimeche, N. Boukid, A. Sakly, and A. Mtibaa, Performance analysis of ZF and MMSE equalizers for MIMO systems, in *7th International Conference on Design & Technology of Integrated Systems in Nanoscale Era* (2012), pp. 1–6
7. On timing offset estimation for OFDM systems. IEEE J. Mag. IEEE Xplore, https://ieeexplore.ieee.org/document/852929
8. L.I. Ting-ting, T. Zheng-rong, Z. Wei-hua, Y. Liu, Improved ACE and ICF low complexity joint algorithm to reduce PAPR of CO-OFDM system. Optoelectron. Lett. **17**, 4 (2021)
9. F. Li, X. Li, J. Yu, Performance Comparison of DFT-SPREAD and pre-equalization for 8 × 244.2-Gb/s PDM-16QAM-OFDM. J. Lightwave Technol. **33**, 227 (2015)
10. C. Nader, P. Händel, N. Björsell, Peak-to-average power reduction of OFDM signals by convex optimization: experimental validation and performance optimization. IEEE Trans. Instrum. Meas. **60**, 473 (2011)
11. U. Das, S. P. Das, S. Kumar, Y. Kumar, S. Singh, and D. Nayak, Performance enhancement of OFDM system by reducing PAPR using DFT spreading technique, in *2016 IEEE International Conference on Recent Trends in Electronics, Information & Communication Technology (RTEICT)* (2016), pp. 886–887
12. X. Chen, J. Cui, W. Ni, X. Wang, Y. Zhu, J. Zhang, S. Xu, DFT-s-OFDM: enabling flexibility in frequency selectivity and multiuser diversity for 5G. IEEE Consum Electron Mag **9**, 15 (2020)
13. A. Sahin, E. Bala, R. Yang, and R. L. Olesen, DFT-Spread OFDM with frequency domain reference symbols, in *GLOBECOM 2017—2017 IEEE Global Communications Conference* (2017), pp. 1–6
14. J. Kim, Y.H. Yun, C. Kim, J.H. Cho, Minimization of PAPR for DFT-spread OFDM With BPSK symbols. IEEE Trans. Veh. Technol. **67**, 11746 (2018)
15. R. Palisetty, K.C. Ray, Oversampled CI-OFDM baseband transceiver architecture and its FPGA prototype: IETE. J. Res. **68**(2), 1023 (2019)
16. D. A. Wiegandt, C. R. Nassar, and Z. Wu, Overcoming peak-to-average power ratio issues in OFDM via carrier-interferometry codes, in *IEEE VTS 54th Vehicular Technology Conference.* Vol. 2, pp. 660–663 (2001)
17. R. Palisetty, K.C. Ray, Multiuser variable rate GO-OFDMA architecture and its FPGA prototype. IEEE Syst. J. **14**, 2455 (2020)
18. X. Chen, A. Li, G. Gao, W. Shieh, Experimental demonstration of improved fiber nonlinearity tolerance for unique-word DFT-spread OFDM systems. Opt Express **19**, 26198 (2011)
19. J. Shi, J. Zhang, N. Chi, J. Yu, Comparison of 100G PAM-8, CAP-64 and DFT-S OFDM with a bandwidth-limited direct-detection receiver. Opt. Express OE **25**, 32254 (2017)
20. J. Shi, J. Zhang, Y. Zhou, Y. Wang, N. Chi, J. Yu, Transmission performance comparison for 100-Gb/s PAM-4, CAP-16, and DFT-S OFDM with direct detection. J. Lightwave Technol. **35**, 5127 (2017)
21. (PDF) Digital Communications, John G. Proakis, 4th Edition|Irfan Jamil-Academia.Edu, https://www.academia.edu/4147685/Digital_Communications_John_G_Proakis_4th_Edition
22. H. Ochiai, H. Imai, On the distribution of the peak-to-average power ratio in OFDM signals. IEEE Trans. Commun. **4**(2), 282–289 (2001)
23. T. Jiang, G. Zhu, Nonlinear companding transform for reducing peak-to-average power ratio of OFDM signals. IEEE Trans. Broadcast. **50**, 342 (2004)
24. T. Jiang, Y. Wu, An overview: peak-to-average power ratio reduction techniques for OFDM signals. IEEE Trans. Broadcast. **54**, 257 (2008)
25. H. Ochiai, On instantaneous power distributions of single-carrier FDMA signals. IEEE Wirel. Commun. Lett. **1**, 73 (2012)
26. H. Ochiai, Exact and approximate distributions of instantaneous power for pulse-shaped single-carrier signals. IEEE Trans. Wirel. Commun. **10**, 682 (2011)
27. M. Sung, S. Kang, J. Shim, J. Lee, J. Jeong, DFT-precoded coherent optical OFDM with hermitian symmetry for fiber nonlinearity mitigation. J. Lightwave Technol. **30**, 2757 (2012)
28. C.-H. Lin, C.-T. Lin, C.-C. Wei, S. Chi, DFT/IDFT-free receiving scheme for spread-OFDM signals employing low-sampling-rate ADCs. Opt. Express **25**, 27750 (2017)
29. J. Zhao and A. D. Ellis, Discrete-fourier transform based implementation for optical fast OFDM, in *36th European Conference and Exhibition on Optical Communication* (2010), pp. 1–3

30. Q. Yang, Z. He, Z. Yang, S. Yu, X. Yi, W. Shieh, Coherent optical DFT-spread OFDM transmission using orthogonal band multiplexing. Opt. Express **20**, 2379 (2012)
31. Y. Fang, L. Tao, and N. Chi, Interleaved subcarrier allocation for DFT-spread OFDM to reduce PAPR, in *2012 17th Opto-Electronics and Communications Conference* (2012), pp. 341–342
32. Y. Liu, Z. Tong, W. Zhang, T. Li, M. Wang, A hybrid algorithm for reducing PAPR of CO-OFDM system based on fast hadamard transformation cascading SLM. Optoelectron. Lett. **17**, 534 (2021)
33. D. Wulich, L. Goldfeld, Bound of the distribution of instantaneous power in single carrier modulation. IEEE Trans. Wirel. Commun. **4**(4), 1773–1778 (2005)
34. Single Carrier FDMA: A New Air Interface for Long Term Evolution. Wiley EBooks. IEEE Xplore, https://ieeexplore.ieee.org/book/8040245

Publisher's Note